Applied Catalysis B: Environmental 241 (2019) 430–441

Contents lists available at ScienceDirect

Applied Catalysis B: Environmental

journal homepage: www.elsevier.com/locate/apcatb

# Effect of metal oxide redox state in red mud catalysts on ketonization of fast pyrolysis oil derived oxygenates

Justin Weber[a], Aaron Thompson[b], Jared Wilmoth[b], Vidya S. Batra[c], Nida Janulaitis[a], James R. Kastner[a,*]

[a] Biochemical Engineering, College of Engineering, The University of Georgia, Athens, GA, 30602 USA
[b] Crop & Soil Sciences, College of Agriculture and Environmental Sciences, The University of Georgia, Athens, GA, 30602, USA
[c] The Energy and Resources Institute, TERI University, Darbari Seth Block, Habitat Place, Lodhi Road, New Delhi 110003, India

ARTICLE INFO

*Keywords:*
Ketonization
Oxygenates
Levoglucosan
Iron oxides
Red mud

ABSTRACT

Iron oxide catalysts derived from red mud were reduced at different temperatures and alkali metals extracted to determine the effect of iron redox state and mixed alkali doping on ketonization of key oxygenates (acetic acid, acetol, formic acid, and levoglucosan) found in fast pyrolysis oil aqueous phase. Hydrogen reduction at 300 °C, compared to 400 and 500 °C, generated the highest level of magnetite and weak and strong acid sites ($NH_3$-TPD), while maintaining base sites ($CO_2$-TPD) in the catalytic material, resulting in the highest acetone and 2-butanone yields from the oxygenate mixture with limited coking. Acid treatment of red mud and subsequent reduction generated higher surface area, yet significantly lower ketonization activity and higher coking activity. This was attributed to the lack of alkali metals, and subsequent base sites generated upon calcination and $H_2$ reduction, when in the presence of levoglucosan. Similarly, poor results were obtained with iron oxides supported on $SiO_2$/$Al_2O_3$ without alkali metals when upgrading the oxygenate mixture. The results indicate the need for a multi-functional catalyst (acid and base sites with oxygen vacancies) when upgrading complex oxygenate mixtures in fast pyrolysis oil.

## 1. Introduction

Several challenges limit the direct use of pyrolysis oil as a liquid fuel, including high oxygen content and acidity, which are caused mainly by the oxygenates present (particularly acetic acid, furfural, acetol, levoglucosan, and methoxy phenolics from lignin). A catalytic strategy for converting these oxygenates into useful products is needed. Many strategies for accomplishing this goal have been proposed in literature, but most suffer from at least one critical issue, such as high processing cost (high pressure $H_2$ requirements), deactivation of expensive catalysts (coke formation/poisoning), or inadequate conversion to desired products (poorly active/selective catalysts). Catalytic ketonization of water extracted bio-oil using metal oxide catalysts is one upgrading strategy of interest, because this process removes lignin derived compounds, converts oxygenates to stable, higher value products without expensive noble metals or hydrogen requirements. Several studies have demonstrated that inexpensive iron oxide catalysts prepared from red mud bauxite refining solid waste can convert bio-oil oxygenates to more valuable products with greater energy density and stability [1–5]. Previous studies with red mud have been conducted in small batch reactors, and there is insufficient research in the literature investigating the use of red mud to convert bio-oil oxygenates in continuous systems. One recent study has demonstrated ketonization of aqueous extracted bio-oil using red mud in a continuous reactor system [4]. In this study, red mud showed ketonization activity similar to that of $CeZrO_x$ [6], and did not experience significant coke formation due to the presence of levoglucosan [4]. The stability, cost, and abundance of iron oxide catalysts prepared from red mud provide rationale for further study of these catalysts in continuous reactor systems. The products formed via ketonization of aqueous extracted bio-oil can be further upgraded via condensation and hydrogenation to drop-in fuels.

Many oxide catalysts have been found to be active in ketonization reactions, including $Fe_3O_4$, $Al_2O_3$, MgO, $TiO_2$, ZnO, and $Cr_2O_3$ [7,8]. There is still some debate in the literature concerning ketonization reaction mechanisms for different oxide catalysts. Several mechanisms have been proposed that involve either the formation of alkylidene or ketene intermediates [3,8]. For iron oxide catalysts, ketonization is believed to take place through the initial dehydration of a carboxylic acid to its corresponding ketene, which reacts quickly with another carboxylic acid to form a ketone [3]. It is theorized that the Lewis acid

* Corresponding author.
*E-mail addresses:* AaronT@uga.edu (A. Thompson), vidyasb@teri.res.in (V.S. Batra), jkastner@engr.uga.edu (J.R. Kastner).

https://doi.org/10.1016/j.apcatb.2018.08.061
Received 19 June 2018; Received in revised form 19 August 2018; Accepted 23 August 2018
Available online 10 September 2018
0926-3373/ 

sites stabilize surface carboxylates [9]. Thus, reducibility and density of Lewis acid sites are important characteristics of metal oxides used for ketonization.

Several metal oxides have been studied for ketonization of oxygenates in water extracted bio-oil including $CeO_2$, $TiO_2$, $Fe_3O_4$, and $La_2O_3/ZrO_2$ [4,6,10,11]. The use of these metal oxides for bio-oil upgrading is especially attractive because of their significantly lower cost than noble metals. In addition, metal oxides are generally more resistant to deactivation than noble metals. [12] However, a major challenge of the use of metal oxides is that they generally suffer from lower activity and selectivity than more expensive commercial catalysts. A recent study conducted at Pacific Northwest National Laboratory evaluated a series of catalysts for ketonization activity. Reactions were conducted in a packed bed reactor system at 300 °C, 1350–1400 psi, and WHSV = 0.13–0.37 $h^{-1}$. Out of 25 catalysts evaluated, $La_2O_3/ZrO_2$ achieved the highest reaction rate (0.15 mmol/g-cat/hr), conversion (25–40%), selectivity (45%) over the course of a 150- hour continuous reaction using acetic acid in water.10] However, lower activity was reported using "real feed" derived from biomass.

In another recent study, $CeZrO_x$ catalyst was used to ketonize a model compound mixture of acetic acid, acetol, furfural, and levoglucosan in a continuous reactor system [6]. This study explored how the presence of $CeO_2$, $TiO_2$, and $ZrO_2$ affected activity and stability of the catalyst. Lewis sites on both $CeO_2$ and $TiO_2$ served as catalytic centers by stabilizing surface carboxylates, allowing them to pair. The addition of $ZrO_2$ disrupted the crystal structure of $CeO_2$, increasing the reducibility and thus the activity of the $CeO_2$. The presence of $ZrO_2$ also gave rise to aldol condensation activity and stabilized the catalyst, which would otherwise deform at high temperatures. However, high levels of $ZrO_2$ may decrease the Lewis site density to a point at which carboxylate species do not pair, decreasing activity. Based on these theories, a ceria zirconia catalyst with composition $Ce_{0.5}Zr_{.0.5}O_2$ was selected for optimal ketonization activity, aldol condensation activity, and catalyst stability. This catalyst showed nearly 100% conversion of carboxylic acids and 40% selectivity in a packed bed reactor system [6]. These results demonstrate how the presence of promoting metals increased catalyst stability, conversion, and ketone selectivity. However, levoglucosan caused severe plugging of the reactor system due to thermal polymerization and had to be diluted to maintain operation of the packed bed reactor system.

One of the main challenges of upgrading bio-oil through HDO is catalyst deactivation through coke formation and poisoning. Coke formation is common when dealing with highly unsaturated substrates, like those found on bio-oil. Increasing $H_2$ pressure generally reduces coke formation but can significantly increase processing costs. In addition, the presence of inorganics in bio-oil, particularly sulfur and phosphorous can poison noble metal catalysts [13]. Iron oxides are of significant interest because they are far less expensive than noble metals and more resistant to deactivation. Many studies have demonstrated the activity of iron-based catalysts for hydrodeoxygenation. One study demonstrated the selective hydrogenation of acetic acid over a series of non-reduced and pre-reduced iron oxide catalysts. Pre-reduction of pure $Fe_2O_3$ catalyst using $H_2$ at 450 °C resulted in partial reduction of $Fe_2O_3$ (hematite) to metallic Fe (zerovalent), which increased selectivity for acetaldehyde formation from acetic acid [7]. It was theorized that the reaction takes place on the oxide phase via the reverse Mars-van Krevelen mechanism. First, hydrogen reduces the metal oxide resulting in oxygen vacancy sites. A carboxylic acid then binds to a vacancy site which is re-oxidized by an oxygen atom on the binding carboxylic acid. Activated hydrogen chemisorbed on the metal surface reduces the carboxylic acid and the resulting aldehyde desorbs. Hydrogen can then re-reduce the metal oxide, regenerating the vacancy site. Thus, reactions following the reverse Mars-van Krevelen mechanism require reducible oxide sites, hydrogen to reduce and regenerate oxygen vacancy sites, and metal sites that can activate hydrogen on the surface in close proximity to oxygen vacancy sites.

Additional studies have demonstrated the activity of iron-based or doped catalysts for hydrodeoxygenation of lignin pyrolysis vapors and acetic acid ketonization [11,13–16]. In one study, $Fe/SiO_2$ (15 wt%) and Fe/AC (10 wt%) were used to improve the quality of pyrolysis oil by catalyzing hydrodeoxygenation reactions of pyrolysis vapor in- line (before condensation of pyrolysis products) [14,15]. The Fe catalysts were pre-reduced at 500 °C, and then subsequently re-reduced in-situ at 400 °C. Hydrogenated products from lignin included benzene, toluene, xylenes, phenol and cresols. $Fe/SiO_2$ selectively catalyzed hydrogenolysis of C—O bonds while avoiding unwanted cracking and hydrogenation of C—C bonds. The overall quality of the condensed bio-oil was improved significantly. As expected, significant coke formation on the catalyst was observed. Olcese et al. [14] argue that deactivation of the catalyst is not of significant concern, because iron-based catalysts are environmentally friendly and inexpensive. However, the need to frequently regenerate or replace catalysts is considered unfavorable. Recently, magnetite supported on $SiO_2$ was demonstrated to convert acetic acid to acetone at high selectivity (60%) and rates similar to $Ru/TiO_2$ and $CeO_2$ catalysts, with weak to moderate Lewis acid sites as the catalytic center [11]. Interestingly, red mud gave similar ketonization rates when compared to the iron oxide supported materials [11]. Recently, iron doped $CeO_2$ ($Ce_{0.8}Fe_{0.2}O_{2-\delta}$) was shown to significantly improve ketonization of acetic and propionic acids relative to $CeO_2$ or $Fe_2O_3$ alone, reportedly due to the superior redox behavior of this material [16]. Although these results validate the use of iron oxide catalysts for ketonization, little information is available on the effect of other components in the fast pyrolysis oil (e.g., acetol and levoglucosan) and the redox state of red mud on bio-oil catalytic upgrading activity.

Finally, water extraction followed by catalytic ketonization of oxygenates in the aqueous phase as a bio-oil upgrading strategy has been explored as a method to reduce catalytic deactivation. [17] The ketone products of catalytic ketonization can then be hydrogenated to form alcohols and alkanes using a catalyst that exhibits hydrogenation activity. In this work we wanted to determine if an iron-based mixed metal oxide catalyst used to ketonize aqueous phase oxygenates in bio-oil could also hydrogenate the ketone products. Iron oxide catalysts that contained zero valent iron have successfully catalyzed the hydrogenation of acetic acid[7] and thus hydrogenation of the ketone products (e.g., acetone, 2-butanone, cyclopentanones) should be easier, since ketones typically show higher hydrogenation activity than carboxylic acids. [13,18] For these reasons, it was hypothesized that a reduction treatment resulting in a mixture of magnetite and zero valent iron could result in an iron catalyst that is capable of simultaneously ketonizing carboxylic acids and then hydrogenating ketone products. Such a catalyst would provide an inexpensive and effective strategy for upgrading aqueous extracted bio-oil to alcohols and alkanes while retaining carbon and minimizing catalyst deactivation.

## 2. Experimental methods

### 2.1. Catalyst preparation

#### 2.1.1. Red mud

Red mud was obtained from Rio Tinto (Alcan, Canada). The wet slurry was dried at 105 °C for 20 h, and then crushed using a hammer. The resulting granules were sieved into two fractions (0.5–2.0 mm and < 0.05 mm). Particles of size 0.5–2.0 mm were used in experiments.

#### 2.1.2. HCl-treated red mud

Acid pretreatment was conducted by The Energy and Resources Institute (TERI) using the following procedure. Red mud from Belgaum, India (10 g) was dried and sieved (< 200 μm) and then mixed with 190 mL of distilled water. The mixture was stirred for 5 min using a magnetic stirrer. HCl (34 mL, 37%) was then added and stirring was

continued at 95 °C for approximately 8 h (until white residue was obtained). The liquid was separated from the residue and aqueous ammonia was added to the liquid drop-wise while stirring until a pH of 8 was reached. The resulting precipitate was centrifuged and washed with warm distilled water to remove residual chlorine. The separated precipitate was dried at 95–110 °C in an oven for 12 h. This material is referred to as RM-HCl and the material $H_2$ reduced as described below is referred to as RRM-300-HCl.

#### 2.1.3. $Fe/SiO_2$-$Al_2O_3$ (10 wt% Fe)

Nonahydrate $Fe(NO_3)_3$ (36.17 g) was dissolved in 10 mL of deionized water. The dissolved solution was then added drop wise to 45 g of $SiO_2$-$Al_2O_3$ catalyst support (previously calcined at 500 °C for 2 h; 6.5% Al, > 90% 100 mesh fine particles provided by Sigma Aldrich). Deionized water (47 mL) was then added and allowed to soak for 24 h. The wet slurry was then dried at 105 °C for 24 h. The resulting solid was crushed into a fine powder and calcined at 300 °C using an air flow rate of 100 mL/min for 18 h.

#### 2.1.4. Catalyst reduction

Catalysts were loaded into a Parr packed bed reactor system, supported by quartz wool or a steel screen, depending on particle size. Catalysts were then reduced in-situ at 300, 400, or 500 °C using $H_2$ flow of 100 mL/min for 20 h prior to use. The mass of catalyst reduced was between 5–20 grams, according to the corresponding reaction.

### 2.2. Ketonization studies using red mud

Studies were conducted to investigate the catalytic properties of a mixed metal oxide catalyst synthesized from red mud for ketonization of bio-oil oxygenates. Model compound mixtures of acetic acid, formic acid, acetol, and levoglucosan (4% each in $H_2O$) were prepared to represent key oxygenates in water extracted fast pyrolysis oil (FPO) [4]. Reactions were then carried out in a continuous packed bed reactor system using red mud that was pre-reduced at 300 °C, except where noted (RRM-300), different $H_2$ reduced red mud, and an $Fe/SiO_2$-$Al_2O_3$ catalyst [4]. Catalysts were characterized before reduction, after reduction, and after use in continuous reactions. The effect of temperature and W/F (W is catalyst mass; F is mass rate; W/F in h) on catalytic ketonization of the model compound mixture was previously studied by varying the reaction temperature from 350 to 425 °C and varying the mass of catalyst used from 5 to 20 g [4]. The reaction temperature and W/F ratio used in this work was based on this previous study and conducted at 400 °C, a W/F of 1.12 h with 5 g of catalyst for approximately 100 min per run. Gas and liquid products of the reactions were collected and analyzed according to procedures outlined in the methods section.

For comparison of catalyst surface properties after reaction we include catalyst samples from past work which were used to upgrade different sources of FPO, water extracted FPO (southern pine and hardwood) [4,5] and one case of a time on stream (TOS) study using the model compound mixture and RRM-300 [17]. All reactions were performed at atmospheric pressure under continuous conditions as described above, except where noted at a different temperature, pressure, liquid flow rate, or catalyst mass (W/F ratio). The time on stream study was conducted for 7 h using 20 g of RRM-300, resulting in a W/F ratio of 4.85 h (400 °C, 101.3 kPa). Details for these experiments are provided in Table S1 and references [4,5,17].

### 2.3. Reduction pretreatment effect

Three different catalysts were prepared from red mud (RRM-300, RRM-400, RRM-500) via reduction in pure hydrogen at 300, 400, and 500 °C. Catalysts were characterized before and after reduction to determine the effect of reduction temperature on iron valence state, reducibility, base site density, and surface area. Each catalyst was used in a series of ketonization reactions using the model compound mixture and best conditions determined in Section 2.2 (T = 400 °C, P = 101.3 kPa ($N_2$), 5 g catalyst) [4]. HCl-treated red mud were tested for comparison.

### 2.4. Pressure and externally added hydrogen effect

In this step ketonization studies using red mud were conducting at elevated pressures. First, reactions using RRM-300 (T = 400 °C, LHSV = 5.646 1/hr) at varying $N_2$ pressure (101.3 kPa − 4.14 MPa) were conducted. In addition, reactions where hydrogen was added externally (at 101.3 kPa) were also conducted. The purpose of these reactions using RRM-300 was to first understand the effect of total pressure and hydrogen availability on the formation of ketonization products (particularly 2-butanone, 2-pentanone, and cyclopentanones). Subsequent ketonization reactions were conducted using RRM-400 and RRM-500 in pure hydrogen. Due to the presence of zero valent iron in red mud reduced at 400 and 500 °C, it was hypothesized that ketone products (acetone, 2-butanone, and cyclic ketones) could be simultaneously hydrogenated to alcohols. These reactions were conducted at atmospheric pressure, 1.03 MPa, and 2.07 MPa ($H_2$) using the following conditions: T = 400 °C, WHSV = 0.89 g/g-cat/hr, LHSV = 5.65 $h^{-1}$.

### 2.5. Hydrogenation studies using red mud and $Fe/SiO_2$-$Al_2O_3$

These studies explored using RRM and $Fe/SiO_2$-$Al_2O_3$ for simultaneous ketonization/hydrogenation of acetic acid, formic acid, acetol, and levoglucosan. Additional reactions were conducted with RRM and $Fe/SiO_2$-$Al_2O_3$ using ketone model compounds (acetone, 2-butanone, and cyclopentanone) to study hydrogenation only. Red mud and $Fe/SiO_2$-$Al_2O_3$ were pre-reduced at 400 °C and 500 °C and used in hydrogenation reactions using the following conditions: P = 2.07 MPa ($H_2$), reaction temperature of 400 °C, WHSV = 0.1262 $h^{-1}$.

### 2.6. Operation of continuous packed bed reactor system

Ketonization and hydrogenation reactions were performed in a continuous packed bed reactor (PBR) system custom designed by Parr Instrument Company. The reactor consists of a stainless-steel tube with inner diameter of 2.4 cm and length of 38 cm. Catalysts were loaded into the top of the reactor, supported by a stainless-steel screen and quartz wool. The reaction temperature was controlled by a Thermcraft Lab- Temp 1760-watt tube furnace powered by a Parr 4875 Power Controller. When applicable, reduction/pretreatment of the catalyst was conducted for 20 h (in-situ) prior to the reaction. Aqueous model compound mixtures were injected downward into the reactor tube at a rate of 0.5–8 mL/min using a Lab Alliance HPLC pump. A total of 50 g of liquid feedstock was injected for each reaction, resulting in a total reaction time between 6–100 minutes, depending on the liquid flow rate used. Nitrogen/hydrogen were supplied as carrier gases to the reactor head at a rate of 100 mL/min using a Brooks Delta II Smart Mass Flow Controller. Pressure was maintained by an in-line back pressure regulator system. The operator controlled all reactions from a safe location (an isolated control room) using SpecView software. A condenser vessel chilled to 7 °C by a Brookfield TC-602 water bath was used to capture liquid products, which were collected at the end of each reaction for analysis. Gas products were collected for analysis from the reactor exhaust line using 1 L Tedlar bags.

### 2.7. Analysis of liquid and gas products

#### 2.7.1. Gas chromatography/mass spectrometry (GC/MS)

The composition of the liquid products collected from each reaction was determined by GC–MS analysis using a Hewlett-Packard (model HP-6890) gas chromatograph coupled with a Hewlett-Packard mass spectrometer (Model HP-5973). An HP-5 MS column (30 m length with

25 mm internal diameter and 0.25 μm film thickness) was used with the following method: inlet temperature of 230 °C and detector temperature of 280 °C, He flow of 1 mL/min, starting oven temperature of 40 °C for 3 min followed by an 8 °C/min ramp to 250 °C, then held for 5 min. The injection volume used was 1 μL and the spectrometer scan range was 10–350 mass units. Compounds were identified using MSD ChemStation D.03.00.611 and the NIST 2008 database. For select compounds (methylated cyclic ketones, 2-pentanone, and 3-pentanone) concentrations were estimated using quantitative GC/MS analysis using hexanol as an internal standard. A standard stock solution was prepared by adding 30 μL of hexanol (106.17 g/L) to a 200 μL mixture of acetone and methanol (1:1 by volume). A series of 3 standard stock solutions were then prepared by adding 5, 10 and 20 μL of the analyte and 6 μL of hexanol stock solution to a 1:1 acetone/methanol mixture, resulting in a final volume of 611 μL. Standard stock solutions contained 1.043 g/L of hexanol and between 0.7 and 10 g/L of the analyte. Stock solutions were injected in triplicate using the method described above. Three-point standard curves were developed that relate the analyte/hexanol peak area ratio to analyte concentration. To quantify analytes in liquid product mixtures that were collected from each reaction, 6 μL of hexanol stock solution was added to 605 μL of the liquid product mixture resulting in a hexanol concentration of 1.043 g/L. The ratio of analyte to hexanol peak area measured via GC/MS was then used to calculate the concentration of analyte in the liquid product mixture using the three-point standard curves. The concentrations of 2-pentanone and 3-pentanone were estimated using the standard curve for 2-butanone. The fragmentation patterns of linear pentanones and 2-butanone were found to be similar, which provided confidence in the accuracy of this quantification method.

#### 2.7.2. Gas chromatography- flame ionization detection (GC-FID)

For certain compounds (acetone, ethanol, 2-butanone, isopropanol, 2-butanol, cyclopentanone, cyclopentanol), a GC-FID was used for quantitative analysis using an HP Innowax column (30 m × 0.25 mm × 0.25 mm) and an HP 5890 Series II detector using the following method: inlet temperature 230 °C, detector temperature 240 °C, initial oven temperature of 45 °C for 2.5 min followed by a ramp of 10 °C/min for 15.5 min and then held at 200 °C for 3 min. Four-point standard curves (run in triplicate) were generated for each of the compounds listed above. When necessary, liquid samples were diluted to ensure that the measured peak areas fall within the range of the standard curves for each compound (typically 1–10 g/L).

#### 2.7.3. High pressure liquid chromatography (HPLC)

Sugars and some organic acids such as levoglucosan, formic acid, and acetic acid were quantified via high pressure liquid chromatography using a Shimadzu LC-20 AT. This instrument uses a RID-10 A refractive index detector and a Coregal 64-H transgenomic analytic column (7.8 × 300 mm). The flow rate, sample size, and run time were 0.6 mL/min, 5 μL, and 55 min, respectively. The mobile phase was 4 mN sulfuric acid. Samples were analyzed at 6.89 MPa at 60 °C. Samples were injected using an LC-20 AT Shimadzu auto-injector. Four-point standard curves (run in triplicate) were generated for acetic acid, levoglucosan, formic acid, and other water-soluble bio-oil oxygenates. Samples were diluted as needed to ensure that the measured peak area falls within the range of the standard curves for each compound (typically 1–10 g/L).

#### 2.7.4. Gas chromatography-thermal conductivity detection (GC-TCD)

Gas products were collected from the reactor exhaust in 1 L Tedlar bags and quantified using a GC-TCD (Hewlett Packard 5890 Series II) using a Carboxen 1000 column (2.1 mm internal diameter) and the following method: inlet temperature 100 °C, detector temperature 140 °C, initial oven temperature 35 °C for 5 min, followed by a ramp of 20 °C/min for 8.25 min and held at 200 °C for 26.75 min. Standard curves for CO, $CO_2$, $CH_4$, and $H_2$ (Airgas Specialty Gases, Cinnaminson, NJ 08,077) were generated from standard gases (4- point standards, run in triplicate) and used for quantitative analysis.

### 2.8. Catalyst characterization methods

#### 2.8.1. Catalyst rinsing

Catalyst samples were rinsed by washing 2.5 g of sample with an acetone- toluene-methanol mixture (1:1:1 by weight) and filtering using Whatman #4 filter paper under a vacuum. Washed samples were then dried at 105 °C for 4–5 h. Percent tar/coke accumulation on the catalyst was determined by subtracting pre-rinse weight from post- rinse weight then dividing by post-rinse weight.

#### 2.8.2. Thermal gravimetric analysis (TGA)

Catalytic coke formation was determined via Thermogravimetric analysis using a Mettler- Toledo TGA/SDTA 851e. Recovered catalyst samples (~0.5 mg) were heated to 800 °C at 10 °C/min in air (flow rate = 50 mL/min). Catalytic coke accumulation was determined by the change in mass of the sample relative to fresh unreacted catalyst. In some cases where coke plugs (thermal coke) accumulated in-front of the catalyst, the total coke plus tar is reported as the increase in mass recovered relative to the starting amount of catalyst. When coke plugs formed in front of the catalyst, thermal coke was separated from the catalyst and not included in the TGA analysis.

#### 2.8.3. BET/BJH

Catalyst samples were degassed for 3–4 hours in nitrogen at 250–300 °C prior to analysis. A 7- point Brunauer-Emmet-Teller (BET) analysis was used to determine the surface area of catalysts. $N_2$ adsorption was measured over a relative pressure ($P/P_0$) of 0.05–0.35 using a Quantachrome Austosorb-1C. Pore size distribution, total pore volume, and average pore radius were estimated using $N_2$ desorption curves using the Barrett, Joyner, and Halenda (BJH) method.

#### 2.8.4. Elemental analysis

Elemental composition analysis of red mud was conducted at WestCHEM School of Chemistry at the University of Glasgow. Fe, Na, Al, Si, Ca, K, and Mg were quantified using ICP-MS in scan mode. [4] Catalysts were digested in sealed Teflon containers using hydrofluoric and nitric acid in a 400 W microwave for 25 min. Additional elemental analysis in the formed and recovered catalysts were determined at UGA using inductively coupled plasma emission spectroscopy (ICP-OCP) performed on a Spectro Arcos FHS16 AMETEK ICP-OES (samples were digested using concentrated $HNO_3$ following EPA method 3051 A).

#### 2.8.5. Temperature programmed reduction (TPR)

Hydrogen temperature programmed reduction was used to study the valence state of active metals (Fe). TPR was conducted using a Quantachrome Austosorb-1C. Approximately 0.25 g of catalyst sample was suspended in a U-tube between two layers of quartz wool. Samples were subject to nitrogen flow at 185 °C for 30 min in order to desorb any adsorbed gases. Samples were then heated from 60 °C to 800 °C at a rate of 20 °C per minute in $H_2$ (3–5 mol% $H_2$ in $N_2$ at 80 mL/min). TCD signal response versus temperature plots were then used to determine the hydrogen consumption as a function of temperature.

#### 2.8.6. Pulse titration

$H_2$ uptake of active metals was determined via pulse titration using a Quantachrome Austosorb-1C. Approximately 0.2 g of catalyst sample was loading into a U-tube, suspended by quartz wool on both sides. Adsorbed gases were desorbed by flowing helium across the catalyst at 140 °C for 30 min. The furnace was then set to the titration temperature (100 °C for Fe). Nitrogen was then allowed to flow for 20 min at the titration temperature. Titrations were then performed by injecting 100 μL of pure $H_2$. Between 6–12 injections were made until the resulting peaks indicated that hydrogen was no longer being adsorbed.

**Table 1**
Compositional analysis of red mud (RM) and $H_2$ reduced red mud catalyst (RRM).

| Properties | Red Mud | RM-HCl | RRM-300 | RRM-HCl-300 | RRM-400 | RRM-500 |
|---|---|---|---|---|---|---|
| Al, % (dry basis) | 14.4 | 10.2 | 9.4 | 8.83 | 10.6 | 12.4 |
| Ca, % | 4.4 | 0.72 | 2.66 | 0.45 | 2.26 | 2.66 |
| Fe, % | 22.6 | 34.2 | 26.8 | 28.2 | 23.2 | 26.6 |
| Na, % | 14.5 | 0.36 | 5.7 | 0.267 | 4.72 | 5.74 |
| Si, % | 8.6 | 0.965 | 0.066 | 0.217 | 0.052 | 0.0724 |
| K,% | 1.8 | 0.0* | 0.025 | 0.0* | 0.022 | 0.032 |
| Mg,% | 0.4 | 0.082 | 0.053 | 0.033 | 0.046 | 0.051 |
| Acid Sites ($NH_3$-TPD) | | | | | | |
| 200-300 °C, mmoles $NH_3$/g | NP | NP | 0.402 | NP | 0.466 | 0.75 |
| 400-600 °C, mmoles $NH_3$/g | NP | NP | 0.35 | NP | 0.0 | 0.0 |
| Base Sites ($CO_2$-TPD) | | | | | | |
| 100-150 °C, mmoles $CO_2$/g | NP | NP | 0.021 | NP | 0.021 | 0.021 |
| 450-600 °C, mmoles $CO_2$/g | NP | NP | 0.27 | NP | 0.0 | 0.0 |

RM-Red Mud Unprocessed or Reduced; NP – Not performed.
* below detection limit of 0.5 ppm.

For select catalysts, an in-situ reduction step was added (hydrogen flow for 60 min at the desired reduction temperature).

#### 2.8.7. $CO_2/NH_3$ temperature programmed desorption (TPD)

$CO_2$ and $NH_3$ temperature programmed desorption were used to estimate the strength of acid and base sites, respectively for the reduced red mud catalyst. TPD was conducted using a Quantachrome Austosorb-1C. Catalysts were degassed at 250–300 °C for 3 h prior to analysis. Approximately 0.2 g of catalyst sample was loaded into a U-tube, packed between the layers of quartz wool. Samples were then degassed at 185 °C in helium followed by saturation with the adsorbate. For $CO_2$-TPD, samples were saturated with 100% $CO_2$ at 30 °C for 10 min. For $NH_3$-TPD, samples were saturated in 100% electronic grade ammonia at 40 °C for 15 min. Samples were then desorbed with helium (80 mL/min) from 30 to 800 °C at a rate of 10 °C per minute. Desorbed $NH_3$ and $CO_2$ were detected using a TCD. Acid or base site density (μmoles $NH_3$ or $CO_2$/g catalyst) was estimated using an $NH_3$ or $CO_2$ TCD standard curve and calculating the peak areas for $NH_3/CO_2$ desorption via numerical integration (a baseline subtracted chromatogram was used for acid site density estimation). A four-point standard was generated via triplicate pulse injection of known volumes of $NH_3$ or $CO_2$.

#### 2.8.8. Mössbauer spectroscopy

Catalyst samples were analyzed via $^{57}$Fe Mössbauer Spectroscopy to determine the relative abundance of iron redox states (hematite, magnetite, and zero valent iron). This method is further outlined in Tishchenko et al. [19]. Approximately 0.5 g of the unreacted red mud catalyst, reduced red mud reduced at 300 °C (RRM-300), 400 °C (RRM-400), 500 °C (RRM-500), and RRM-300-HCl were loaded and spectra were taken at 140 K for approximately 24 h. In addition, the unreacted red mud was analyzed at 295 K and 4 K. Details on the analysis and fitting methods are reported in previous work [17].

## 3. Results and discussion

### 3.1. Catalyst characterization

Compositional analysis was conducted on untreated and 300 °C-reduced red mud using previously described methods and indicated high levels of iron (22.6%), sodium (14.5%), and aluminum (14.4%) with lower levels of silicon, calcium and titanium (Table 1). Treatment of the red mud with HCl significantly reduced Na, Si, Ti, and K (Table 1). Red mud pre-reduced at 300, 400, and 500 °C were analyzed via Mössbauer spectroscopy to determine the composition of the iron phase. Mössbauer spectra for red mud catalysts indicated that a majority of the iron in the unreduced red mud exists as hematite (Fig. 1) [17]. After reduction at 300 °C, all hematite was converted to magnetite. Increasing reduction temperature to 400 °C results in further reduction of a portion of the magnetite to zero valent iron (~25%). After reduction at 500 °C, a greater portion of the magnetite was reduced to zero valent iron (~47%). Interestingly, when comparing reduced red mud with RRM-HCl and $Fe/SiO_2$-$Al_2O_3$ the latter iron oxides had significantly lower levels of magnetite and higher goethite (FeOOH) levels when reduced at the same temperature (300 and 500 °C – Table 2).

The alkali metals and reduction temperature not only effected the redox state of the iron oxides but altered surface area and pore size

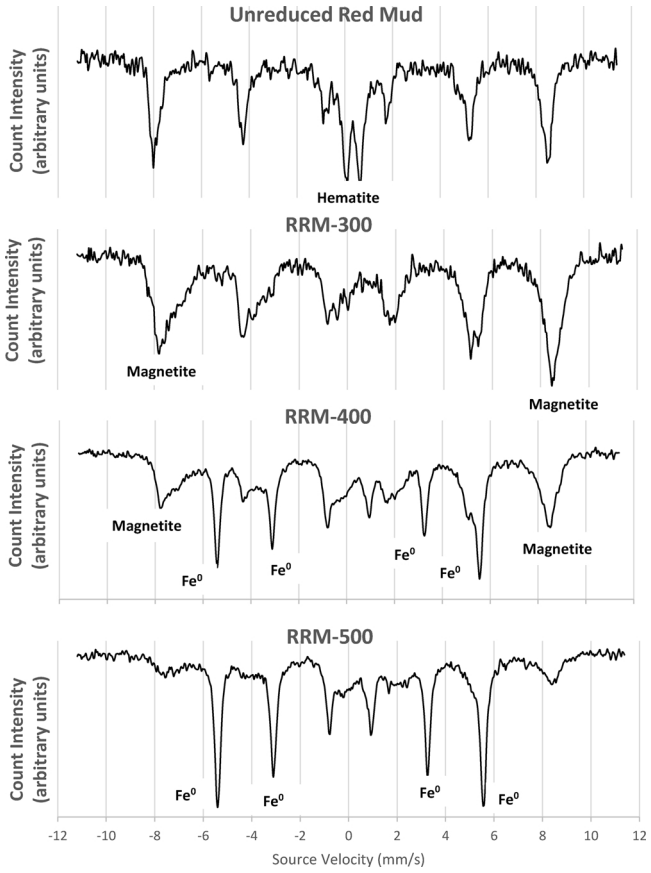


**Fig. 1.** $^{57}$Fe Mössbauer spectra at 140 K of the unreacted Red Mud (top spectra), red mud reduced at 300 °C (middle spectra), reduced at 400 °C (second from bottom spectra), and reduced at 500 °C (bottom). In each spectrum, the black solid line is the total calculated fit, through the discrete data points.

**Table 2**
Physical properties of iron oxides catalysts.

| Properties<br>Catalyst | Surface Area ($m^2$/g) | Pore Volume[a] ($cm^3$/g) | Average Pore Diameter[a] (Å) | Hematite<br>% | FeOOH<br>% | Magnetite<br>% | Fe°<br>% |
|---|---|---|---|---|---|---|---|
| $SiO_2$-$Al_2O_3$ | 405 | 0.415 | 41.0 | NP | NP | NP | NP |
| Fe-SiAl | 405.5 | 0.245 | 24.20 | NP | NP | NP | NP |
| Fe-SiAl-300 | NP | NP | NP | 0 | 48 | 45 | 0 |
| Fe-SiAl-400 | 405.5 | 0.57 | 56.2 | NP | NP | NP | NP |
| Fe-SiAl-500 | NP | NP | NP | 0 | 41 | 27 | 27 |
| RM | 13.3 | 0.017 | 51.8 | 100 | 0 | 0 | 0 |
| RRM-300 | 30.7 | 0.038 | 49.8 | 0 | 14 | 86 | 0 |
| RRM-300-HCl | 224.3 | 0.16 | 28.8 | 0 | 67 | 27 | 0 |
| RRM-400 | 27.0 | 0.040 | 59.6 | 0 | 0 | 75 | 25 |
| RRM-500 | 22.7 | 0.033 | 58.8 | 0 | 0 | 53 | 47 |

RM: Red Mud; RRM: Reduced red mud; NP: Not performed; Bulk Density $SiO_2$-$Al_2O_3$ - 0.46 g/$m^3$; Bulk Density RRM-300 - 0.93 g/$m^3$.
Hematite, FeOOH, Magnetite, and Fe° percentages were estimated from Mössbauer spectroscopy.
[a] Pore volume and average pore size were evaluated at P/Po = 0.72 to 0.88.

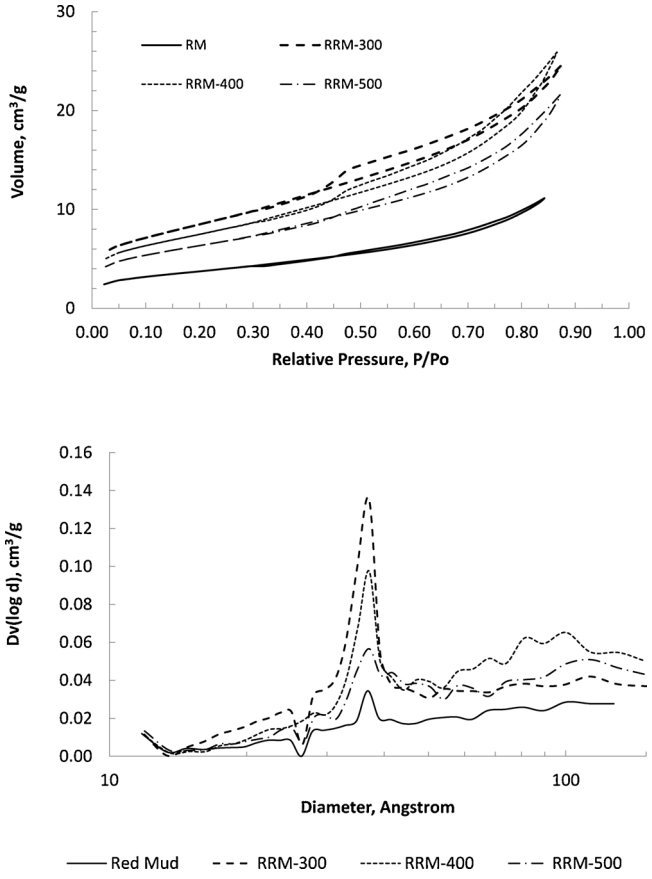


**Fig. 2.** Effect of catalyst reduction temperature on nitrogen adsorption isotherms (top) and pore size distribution (bottom) for red mud. RRM is reduced red mud at 300, 400 or 500 °C.

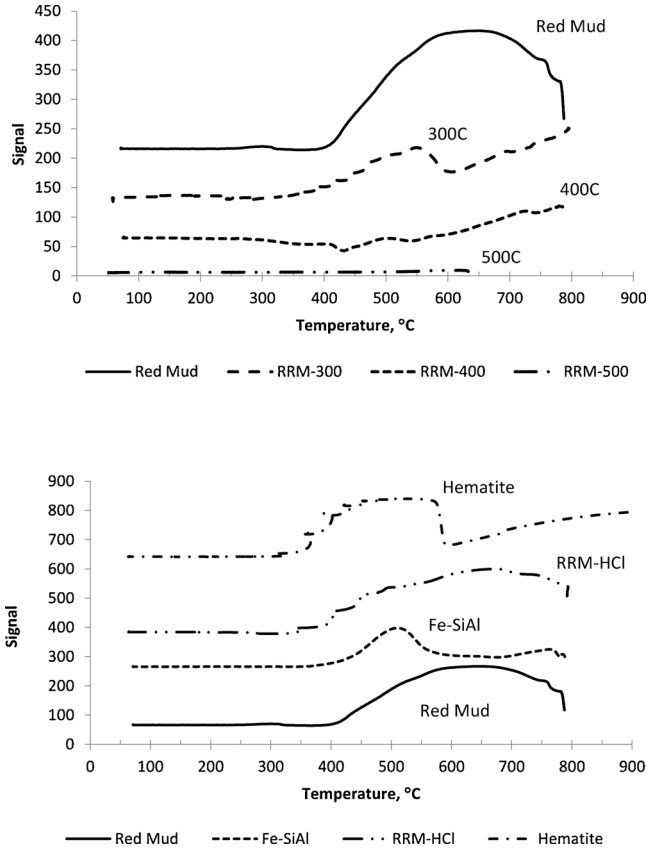


**Fig. 3.** Temperature programmed reduction of red mud reduced with $H_2$ at different temperatures (top) and pure hematite, RRM-HCl, Fe-SiAl, and red mud (bottom). The small loops in signal response for hematite and RRM-HCl samples were due to a non-linear heating profile during these runs. Baselines are offset for clarity.

distribution. Red mud was found to have significantly lower surface area than all other catalysts tested (Table 2). Reduction of red mud at 300 °C for 20 h lead to increases in surface area (from 13.30 to 30.7 $m^2$/g) and pore volume (0.017 to 0.038 $cm^3$/g). This significant change was also apparent in the pore size distribution (via BJH analysis) and $N_2$ adsorption isotherms (Fig. 2); reduction at temperatures > 400 °C lead to a small reduction in surface area and pore volume (Table 2 and Fig. 2).

Hydrogen temperature programmed reduction (TPR) was used to determine the reducibility of the catalyst and estimate the valence state for iron oxides. TCD signal versus temperature plots indicate the amount of hydrogen consumed in the reduction of active metals at temperatures between 60–800 °C. This procedure did not involve standard curves for quantifying hydrogen consumption, and thus comparisons between TPR plots are purely qualitative. Fig. 3 shows TPR profiles for untreated red mud compared with red mud that was pre-reduced in $H_2$ at 300, 400, and 500 °C, as well as other iron oxide catalysts. For red mud a large peak from 400 to 750 °C was observed, likely representing hydrogen consumed in the reduction of hematite and magnetite to zero valent iron. There was a significant reduction in the peak $H_2$ consumption between 400 to 750 °C for RRM-400 and 500, suggesting lower to non-existent levels of hematite (Fig. 3). Mössbauer analysis suggests ~50% of the iron in the unreduced red mud is

hematite and 50% is present as nanoparticulate or substituted goethite. After reduction at 300 °C, however 74% of total iron is present as non-stoichiometric magnetite phases (approximately half Fe in A and B magnetite sites) with the balance as nanoparticulate phases (likely nano-goethite) [17].

Our Mössbauer data suggest the red mud is composed of two primary iron phases, hematite and a nano-scale or highly substituted goethite phase [17]. At 295 K, we resolved a broad sextet with a high field strength and negative quadrapole splitting consistent with crystalline hematite (Bhf = 50.9 T, QS = − 0.1) [17]. Upon reduction at 300 °C, the bulk of the iron is converted to magnetite (Fig. 1) as seen previously by Costa et al. and Weber et al. [17,20], and when reduced in the presence of $H_2$ at 400 and 500 °C a portion of the iron is reduced further to Fe° (Fig. 1) [17,20]. It is clear that $H_2$ reduction at temperatures greater than 400 °C, lead to a reduction in surface area (Table 2), a reduction in pore volume (Fig. 2), an increase in the zero valent iron (Fig. 1), but as described next significantly altered the acid and base site density in the material.

Ammonia TPD indicated the presence of acid sites on the reduced red mud which was dependent on the $H_2$ reduction temperature. The red mud reduced at 300 °C had two acid sites, one at 240 °C (weak acid) and the other at 505 °C (strong acid). Upon reduction at 400 and 500 °C, the strong acid site disappeared, and the weak acid sites increased in density (based on apparent peak area increase – Fig. 4 and Table 1). The

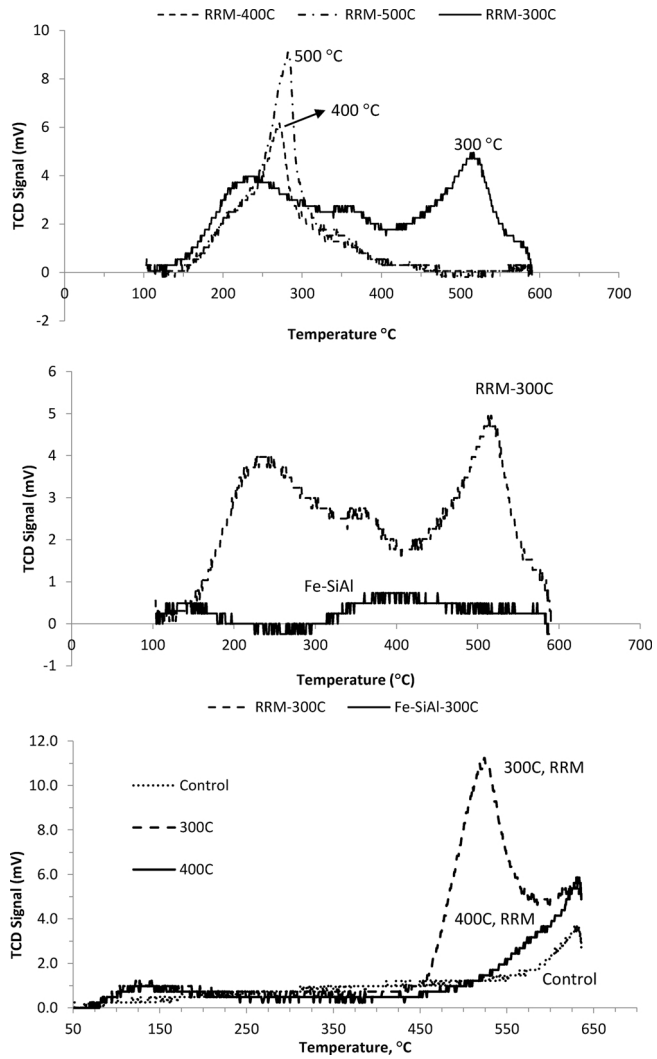


**Fig. 4.** Ammonia (top two) and $CO_2$ (bottom) temperature programmed desorption of differently reduced iron oxide materials. RRM is reduced red mud.

$Fe/SiO_2$-$Al_2O_3$ material did not apparently have acid sites since the ammonia peaks were quite small relative to reduced red mud [at 400 and 500 °C as well, data not shown). Interestingly, a $CO_2$ desorption peak was observed at 520 °C for the 300 °C reduced red mud but disappeared upon reduction at 400 °C (similar results were observed for RRM-500 °C). We did not test the $Fe/SiO_2$-$Al_2O_3$ material for $CO_2$ TPD, since we did not anticipate the presence of base sites. As discussed later the presence of magnetite, and both strong acid and base sites in the 300 °C reduced red mud may have played a significant role in its activity and selectively of products relative to the RRM-HCl and $Fe/SiO_2$-$Al_2O_3$ materials.

### 3.2. Effect of reduction treatment of red mud on ketonization activity

The aqueous phase of fast pyrolysis oil (FPO) contains carbohydrates (e.g., levoglucosan), aldehydes, ketones, and carboxylic acids. For example, FPO generated from pine generates an aqueous phase with 78 g/L of levoglucosan [21]. Water extraction studies of FPO indicate yields from 80 to 90% for levoglucosan, glycoaldehyde, acetol, and acetic acid from pine bio-oil [22]. Previous continuous processing of fast pyrolysis oil oxygenates using RRM indicated reaction rates similar to those reported for $CeZrO_x$ (3–11 vs. 8 mmol/g-cat/h), and acetone selectivity from 8 to 17% [4,6]. Levoglucosan reactivity was lower than the other compounds, but severe coking was not observed and acetone was formed [4]. Moreover, recent limited time on a stream (TOS) studies observed no measurable decline in conversion of acetol, formic acid, and levogluocsan, and a small decline in acetic conversion, suggesting minimal leaching of active sites and deactivation using RRM (all using red mud reduced at 300 °C) [17]. Given these previous results we wanted to explore the possibility of simultaneous ketonization (acid and base sites) and hydrogenation (zero valent iron site) using reduced red mud. We reasoned that a reduction treatment resulting in a mixture of magnetite and zero valent iron could result in an iron catalyst capable of simultaneously ketonizing carboxylic acids and then hydrogenating ketone products. Such a catalyst would provide an inexpensive and effective strategy for upgrading aqueous extracted bio-oil to alcohols and alkanes while retaining carbon and minimizing catalyst deactivation.

Subsequently, the effects of $H_2$ reduction treatment temperature on catalyst activity was measured. Reactions were conducted in the packed reactor at 400 °C, 101.3 kPa ($N_2$), a WHSV of 0.89 g/g-cat/hr, and a LHSV of 5.65 $h^{-1}$. In addition to red mud reduced at three different temperatures, $Fe/SiO_2$-$Al_2O_3$ reduced at 300 °C and HCl-treated red mud (reduced at 300 °C) was tested for comparison. Fig. 5 shows the yield, selectivity, and space time yields with respect to primary products (acetone, 2-butanone, and cyclic ketones) for each catalyst correlated with the estimated magnetite levels. The best results were seen using RRM-300, which achieved acetone, cyclic ketones, and 2-butanone space time yields of 67, 40, and 15 g/L-cat/h, respectively. The HCl-treated red mud achieved similar yields compared to $Fe/SiO_2$-$Al_2O_3$ and RRM-500. But this material generated lower acetone and 2-butanone yields compared to RRM-300, although it had much higher surface area. Low conversions of acetic acid (1.3% for HCl-RRMl and 0% for $Fe/SiO_2$-$Al_2O_3$-300; Fig. S1) seen using HCl-RRM and $Fe/SiO_2$-$Al_2O_3$ were probably due to the low levels of magnetite ($Fe_3O_4$) and the lack of coordinated Lewis acid and Bronsted basic sites in these materials that reportedly catalyze the ketonization reaction. [11,26,27], Acid treatment of the red mud extracted alkali metals during the activation process and may have resulted in the significantly different structure upon $H_2$ reduction compared to red mud [23]. Magnetite reportedly has higher ketonization activity than hematite [26] and a key active site is thought to be a Lewis acid [11]. Strong evidence has recently been reported that Lewis acid sites in $Fe_3O_4$ supported on $SiO_2$ catalyze acetic acid ketonization [11]. When doped with alkali metals, such as Na, the metal oxide $ZrO_2$ increased ketonization activity and acetone yield, reportedly due to stabilization of the metal oxide [28].

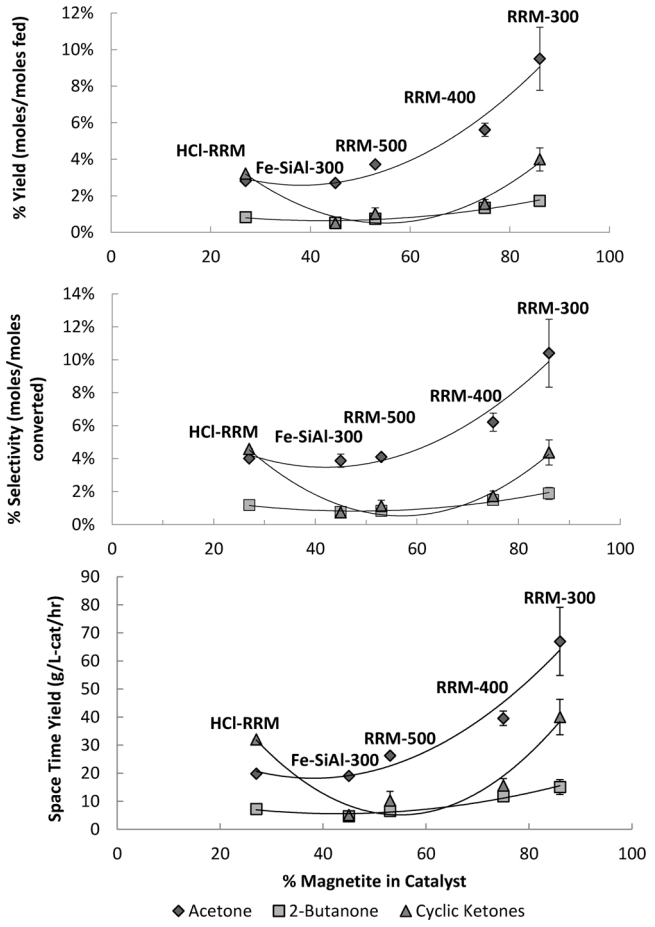


**Fig. 5.** Effect of catalyst redox state on yield, product selectivity, and Space Time Yield using iron oxide catalysts (P = 101.3 kPa (14.7 psig), 400 °C, W/F = 1.12 h, 5 g cat.). Note: 86% magnetite is RRM-300, 75% is RRM-400, 53% is RRM-500, 27% is HCl-RRM, and 45% is Fe-SiAl.

Acetic acid was determined to be the rate limiting reactant for the catalysts, since the fractional conversion of acetic acid (~75%, except for RRM-HCl and Fe/$SiO_2$-$Al_2O_3$) was lower than that of all other reactants (100%) across all catalysts (Fig. S1). Carbon recovery in the liquid phase decreased with increasing catalyst reduction temperature (Fig. S2) and a clear decline in selectivity for ketone products with increasing reduction temperature of red mud was observed (Fig. 5). We attribute this to the smaller amounts of magnetite (as well as lower levels of strong acid sites) present in RRM-HCl and Fe/$SiO_2$-$Al_2O_3$, which is theorized to be the active metal for ketonization. Large acetaldehyde peaks were detected via GC-FID in products from reactions using RRM-400 and RRM-500, suggesting an increased conversion of acetic acid to acetaldehyde via the reverse Mars-van Krevelen mechanism and may explain the lower acetone yields and carbon balance in reactions using RRM-400 and RRM-500 (Fig. S3).

Evidence in the literature suggests that the presence of zero valent iron in reduced red mud could promote hydrogenation activity [7]. In addition, previous studies indicate that decomposition of formic acid in bio-oil can provide an internal source of hydrogen needed for hydrogenation reactions to take place [1]. Thus, it was theorized that simultaneous ketonization and hydrogenation may be possible when using red mud reduced at higher temperatures due to higher levels of Fe°. Reduced red mud containing zero valent iron showed similar conversion of acetic acid, formic acid, acetol and levoglucosan, but showed lower selectivity for ketone products. This suggests that reactants or products were converted to coke. Although TGA analysis indicated little catalytic coke formation on all three red mud catalysts (no measurable coke via TGA-Fig. S4 and Table S1), large chunks of thermal coke were observed in reactions using RRM-400 and RRM-500. Higher reduction temperatures led to an increase in the total mass of solids collected after reactions (4–12%, Table S1). This suggested that coke formation increased with increasing reduction pretreatment temperature, but this coke does not seem to form uniformly on the surface of the catalysts. We speculate that the acetaldehyde formed due to the presence of Fe° in the RRM 400 and 500 catalysts undergoes rapid oligomerization and condensation reactions generating thermal coke. Work by Gayubo et al. [29] using HZSM-5 to upgrade individual oxygenates found in fast pyrolysis oil indicated significant catalyst deactivation due to coke formation when treating acetaldehyde, compared to alcohols, acetone, butanone, and acetic acid (400 °C) [29]. They attributed this to the rapid condensation and oligomerization reactions of acetaldehyde in the reactor and on acid sites leading to the formation of both thermal and catalytic coke [29].

Finally, none of the expected hydrogenation products (isopropanol, 2-butanol, cyclopentanol, ethanol, methanol) were observed. Interestingly, hydrogen was detected in the gas products (3 mol%) using RRM-500, but not RRM-300 or RRM-400. It is theorized that this hydrogen was generated through the decomposition of formic acid. The presence of hydrogen may promote the hydrogenation of ketone products to alcohols and alkanes. However, it is unlikely that significant hydrogenation of ketone products could take place under the low hydrogen partial pressure conditions in these experiments.

### 3.3. Effect of total pressure on ketonization

At this point our thoughts were that the presence of hydrogen measured in the gas phase products in reactions using RRM-500 supported the hypothesis that hydrogen is produced internally via decomposition of formic acid. However, the very low hydrogen partial pressure observed (3.04 kPa) was unlikely to lead to significant hydrogenation of ketone products. It was theorized that increasing hydrogen partial pressure may lead to simultaneous hydrogenation of ketone products to alcohols. To test this hypothesis, a series of experiments were conducted that tested the effect of total pressure on ketonization/hydrogenation of carboxylic acids using red mud reduced at 300 °C (400 °C, LHSV = 5.646 1/h). Total reaction pressure was varied from atmospheric pressure to 600 psi (0.101–4.14 MPa) using nitrogen increasing the partial pressure of internally generated hydrogen, if present.

Increasing total pressure from atmospheric pressure to 1.03 MPa led to an increase in 2-butanone selectivity, but further increase in pressure showed no significant trends (Fig. 6). Total conversion of reactants was not significantly affected by total pressure. However, cyclic ketone selectivity decreased significantly when increasing total pressure above atmospheric pressure. Quantitative GC/MS analysis indicated increasing levels of linear pentanones (2-pentanone, 3-pentanone, and various methylated pentanones – Fig. 6). It is possible that increasing total pressure increased the availability of internally generated hydrogen, which lead to increased conversion of acetic acid to acetaldehyde via the reverse Mars-van Krevelen mechanism (Fig. S3). Acetaldehyde could then be converted to 3-pentan-2-one via condensation with acetone and further hydrogenated to 2-pentanone (Fig. S5). A shift in selectivity from acetol to propylene glycol rather than pyruvaldehyde may explain the decrease in cyclic ketones and increase in 3-pentanone and 2-butanone, although the exact mechanism is unclear. It is theorized that 3-pentanone is generated via hydrogenation of acetol to propylene glycol, followed by pinacol arrangement to propanal, followed by oxidation to propanoic acid and ketonization to form 3-pentanone [24]. The carbon balance (Fig. 6) shows that increasing total pressure lead to significantly reduced gas phase carbon generation ($CO_2$ and CO). The decrease in recovered carbon at higher pressures was attributed to increased coke formation. Similar to the findings using RRM-400 and 500 °C at atmospheric pressure, coke seemed to

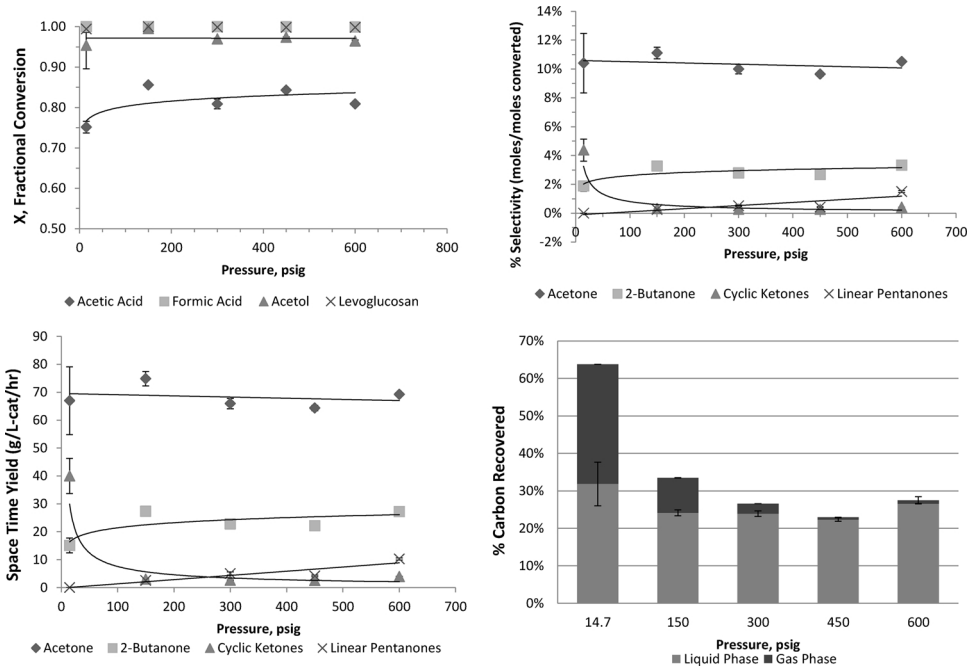


**Fig. 6.** Effect of pressure (0.101–4.14 MPa [14.7–600 psig]) on conversion, product selectivity, space time yield, and carbon recovery using RRM-300C catalysts (400 °C, W/F = 1.12 h, 5 g cat.).

form into chunks near the top of the catalyst bed rather than on the surface of catalyst particles throughout the bed. The total mass of coke + tar collected after each reaction ranged from 0.5, 0.4, and 0.2 g for 1.03, 2.07, and 3.1 MPa respectively (coke + tar was not collected at 101.3 kPa or 4.13 MPa; Table S1). We acknowledge probable error in recovery of the coke particles at the higher pressures (1–4 MPa), since the carbon recovery indicates that coke should increase with pressure. Regardless, large plugs of coke were observed for reactions at 1.03 and 2.07 MPa, but no plugging was observed at atmospheric pressure. In addition, no hydrogen was detected in the gas products, indicating that any hydrogen generated via formic acid decomposition was immediately consumed.

### 3.4. The effect of externally added hydrogen

Previously, it was theorized that increasing the total pressure would increase the availability of internally generated hydrogen for hydrogenation of ketones to alcohols. However, none of the expected hydrogenation products from acetone, 2-butanone, or cyclopentanone were detected. To further explore the potential simultaneous ketonization/hydrogenation activity of red mud, hydrogen was added externally as a carrier gas. Past work indicated that hydrogen may have a role in the formation of several products including 2-butanone, 2-pentanone, and cyclopentanone [4,6,14,15,17]. To further understand this, the best reaction conditions from the ketonization experiments with red mud were repeated using hydrogen instead of nitrogen as a carrier gas [RRM reduced at 300 (P = 101.3 kPa), 400 and 500 °C, pure $H_2$ gas, WHSV of 0.89 g/g-cat/hr, LHSV of 5.65 $h^{-1}$, feed of 4% acetic acid, formic acid, levoglucosan, and acetol].

A comparison between ketonization reactions using $H_2$ and $N_2$ as a carrier gas at atmospheric pressure showed no significant differences between acetone or 2-butanone yields (Fig. 7). Significantly lower cyclic ketone yields were observed for reactions using externally added $H_2$. In addition, 2-pentanone and 3-pentanone peaks were observed via GC/MS in reactions using $H_2$ (atm). The shift in selectivity from cyclic ketones to 2-pentanone and 3-pentanone was also observed in ketonization reactions at elevated nitrogen pressure (Fig. 6), suggesting that increasing total pressure ($N_2$) or adding external hydrogen have a similar effect on product selectivity. Interestingly, increasing pressure from atmospheric pressure to 1.03 MPa resulted in a significant increase in acetone and 2-butanone space time yields using both RRM-400 and RRM-500 (Fig. S6). These observations are consistent with the previous results, where the effect of increasing nitrogen pressure was tested. It is apparent that increasing reaction pressure (regardless of carrier gas) from atmospheric pressure (14.7 psi) to 1.03 MPa (150 psi) increases the conversion of acetic acid and acetol, which leads to higher acetone and 2-butanone space time yields (Figs. 6 and S6). Increasing pressure beyond 1.03 MPa (150 psi) seems to have no significant effect on conversions of reactants or ketone product yields. These observations support the original hypothesis that increasing total pressure shifts selectivity from cyclic ketones to linear pentanones by increasing the availability of internally generated hydrogen. The addition of hydrogen also resulted in larger acetaldehyde peaks (identified via GC/FID, but not quantified). This supports the hypothesis that $H_2$ increases selectivity for acetaldehyde from acetic acid via the reverse Mars van Krevelen mechanism.

### 3.5. Ketonization of carboxylic acids using $Fe/SiO_2$-$Al_2O_3$

Ketonization activity of $Fe/SiO_2$-$Al_2O_3$ was compared with that of reduced red mud at identical reaction conditions. Analysis of liquid products indicated that $Fe/SiO_2$-$Al_2O_3$ forms the same major products as reduced mud in previous experiments suggesting the ketonization pathway proposed for red mud is similar for $Fe/SiO_2$-$Al_2O_3$. However, $Fe/SiO_2$-$Al_2O_3$ showed significantly lower ketone yields than red mud (Fig. 5) and little to no acetic acid was converted by $Fe/SiO_2$-$Al_2O_3$. However, acetol, levoglucosan, and formic acid were not detected in the liquid products and appeared to have been completely converted. The loss of carbon can be explained by the formation of coke. TGA analysis on spent $Fe/SiO_2$-$Al_2O_3$ indicated high levels of coke (~4%; Table S1 and Fig. S4). Additionally, a solid plug of coke (approximately 0.1 g) was observed near the top of the $Fe/SiO_2$-$Al_2O_3$ catalyst bed that was not seen in experiments using red mud (except for RRM-400 and 500). This plug was likely the result of thermal polymerization of

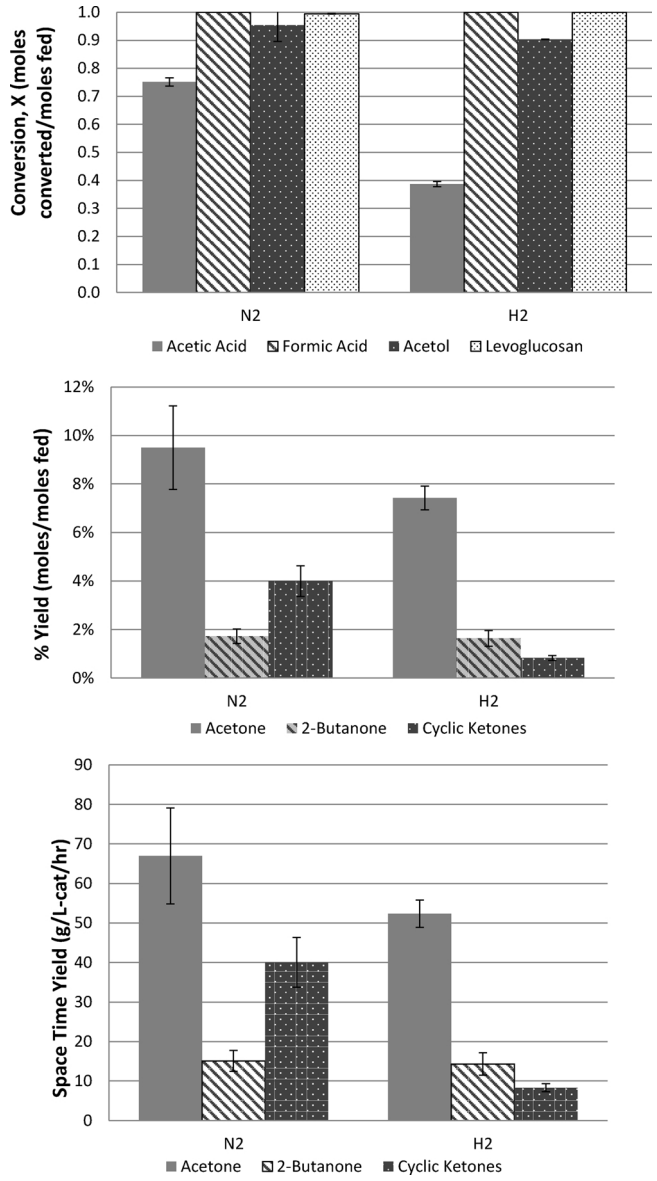


**Fig. 7.** Effect of hydrogen (P = 101.3 kPa) on conversion, product selectivity, and space time yield using RRM-300 C catalyst (400 °C, W/F = 1.12 h, 5 g cat).

levoglucosan (LG). The resistance to coke formation exhibited by red mud (RRM-300C) may be due to the presence of promoting alkali metals (e.g., Ca, Na and K) and strong base sites as indicated in the $CO_2$-TPD (Fig. 4) [25]. Limited work with pure levoglucosan (LG) and metal oxides in ketonization reactions exist. Mesoporous molecular sieves with the lowest number of Bronsted acid sites with Lewis acid sites present converted LG to furfural, generating the lowest coke levels [30]. The presence of potassium during levoglucosan pyrolysis significantly altered the reaction pathway forming acetic acid, acetol, dianhydrosugars, and cyclopentenone derivatives, as well as char [31]. Except for the dianhydrosugars and char (or coke) these products are similar to those reported for ketonization of levoglucosan using reduced red mud (RRM-300C) [4]. Thus, coke formation that partially blocks active sites on $Fe/SiO_2$-$Al_2O_3$, potentially due to lack of base sites, is one explanation for the lower ketonization activity observed. In addition, $H_2$ pulse titration of $Fe/SiO_2$-$Al_2O_3$ indicated much lower dispersion for $Fe/SiO_2$-$Al_2O_3$ compared to RRM (Table 3). The low concentration of iron exposed on the surface of the $Fe/SiO_2$-$Al_2O_3$ catalyst provides another rationale for the low ketone yields and selectivity that were observed.

**Table 3**
Hydrogen uptake and dispersion analysis of iron oxide catalysts.

| Properties Catalyst | Surface Area ($m^2$/g) | Pore Volume ($cm^3$/g) | Average Pore Diameter (Å) | Specific $H_2$ Uptake | | Dispersion* % |
|---|---|---|---|---|---|---|
| | | | | µL/g-cat | µL/g metal | |
| Fe-SiAl-400 | 405.5 | 0.57 | 56.2 | 26 | 260 | 0.13 |
| Fe-SiAl-500 | NP | NP | NP | 99.5 | 995 | 0.50 |
| RRM-300 | 30.7 | 0.038 | 49.8 | NP | NP | NP |
| RRM-400 | 27.0 | 0.040 | 59.6 | 215 | 1918 | 1.0 |
| RRM-500 | 22.6 | 0.033 | 58.8 | 428 | 3820 | 2.0 |

RRM: Reduced red mud; NP: Not performed.
* calculated from $H_2$ pulse titration at 100 °C.

### 3.6. Catalyst surface properties after reaction

Catalyst deactivation can occur by poisoning, sintering, coking, active site restructuring, and leaching. Sintering, active site restructuring, and coking can lead to changes in catalyst surface area and pore volume. Analysis of recovered catalysts relative to fresh catalyst, did indicate significant reduction in surface area and pore volume, and the formation of coke which was dependent on the type of catalyst and components in the feed (Figs. 8, S4, and Table S1). Catalytic coke (formed on catalyst measured by TGA) and thermal coke (plugs formed in front of catalyst and tar) were most notable and surface area reduction the largest when upgrading commercial FPO (Figs. 8, S4, and Table S1). TGA analysis of RRM catalyst treating commercial bio-oil indicated significant mass loss or carbon burn off from 200 to 600 °C, indicating the formation of catalytic coke (Figs. 8, S4, and Table S1). This was most probably due to the presence lignin oligomers, methoxy phenolics, and furfural [5]. When the FPO was fractionated and the aqueous phase upgraded, there was a significant reduction in thermal and catalytic coke (Fig. 8). TGA analysis of RRM catalyst treating water extracted FPO is presented in Kastner et al. [4]. This aqueous phase fraction did have higher levels of levoglucosan (~50 g/L) and acetate (~50 g/L) as well as 5-hydroxy methylfurfural (5-HMF) and furfural compared to mixed oxygenate experiments.[4] Eliminating lignin oligomers, phenolics, 5-HMF and furfural from the feedstock further reduced the formation of coke, although there were still significant reductions in surface area and pore volume (Fig. 8). The most notable exceptions were the formation of coke on RRM-400 and 500, HCl-RRM, and $Fe$-$SiO_2/Al_2O_3$ in the presence of levoglucosan (Figs. 8 and S4). To a smaller extent than commercial or water extracted bio-oil, catalytic coke was also observed using HCl-RRM 300 and $Fe/SiO_2/Al_2O_3$ and the mixed oxygenate stream (Figs. 8, S4, and Table S1). Finally, a ketonization time on stream (TOS) study (~7 h) of the oxygenate mixture (acetic acid, formic acid, acetol, levoglucosan) using RRM-300 maintained constant yields of acetone, 2-butanone, and cyclic ketones, with only a 4% decline in acetic acid conversion [17]. During this period there was no measureable formation of coke as indicated by TGA analysis or weight gain (Figs. 8, S4, Table S1). However, relative to fresh catalyst, surface area and pore volume of the recovered catalyst decreased 38% and 26% respectively (Fig. 8). This change in surface area may have been due to sintering or oxidation of the RRM, suggesting that prolonged use > 7 h could lead to significant deactivation. Lu et al. [16] recently performed a TOS study (5 h, 350 °C) using an iron doped cerium oxide catalyst ($Ce_{0.8}$ $Fe_{0.2}O_{2-\delta}$) to ketonize acetic acid to acetone. [16] An approximate 10% reduction in acetic acid conversion was observed without coke formation, yet activity could be regenerated in-situ by hydrogen reduction, indicating the need to maintain a defined redox state for activity. Our results indicate the need to separate coke forming reactants from FPO (or design a process to separate them from biomass during pyrolysis). If catalytic coke does form on RRM with prolonged use then a two-phase regeneration process may be

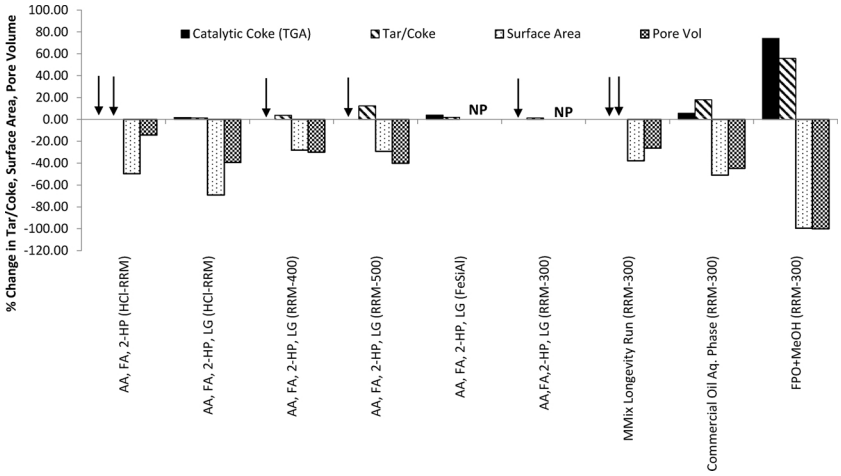


**Fig. 8.** Catalyst surface properties after reaction with oxygenate mixtures, fast pyrolysis oil (FPO), and the aqueous phase of FPO [reaction conditions are reported in Table S1]. The arrows indicate values below detection. NP indicates not performed. AA is acetic acid; FA is formic acid; 2HP is 1-hydroxy-2-propanone or acetol; LG is levoglucosan. All runs were ~100 min except for the MMix Longevity Run (RRM-300 using AA, FA, 2-HP, LG) time on stream study for ~7 h.

needed; e.g., oxidation to remove coke followed by reduction to regenerate the magnetite phase. More prolonged TOS studies are required to fully understand the mechanisms of RRM deactivation, since we have not ruled out alkali metal leaching or acid/base site poisoning as possibilities or confirmed oxidation of magnetite to hematite as a deactivation mechanism. Future development of in-situ regeneration methods would depend on identification of deactivation mechanisms.

## 4. Conclusions

The results indicate that conversion of oxygenates in aqueous extracted bio-oil to higher value compounds with greater energy density and stability is possible in a continuous process using reduced red mud (RRM) as a catalyst. Previous work using RRM-300C indicated reaction rates similar to those reported using $CeZrO_x$ [6], but no significant reactor plugging was observed in the presence of levoglucosan and the reaction/catalyst was stable in time on stream studies (7 h), again in the presence of levoglucosan [4,17].Yet the reason for this stability was unclear. In this work, increasing catalyst reduction pre-treatment temperature led to lower ketone selectivity and yield, and higher coke levels. This was likely due to a lower concentration of magnetite, a lower density of strong basic sites due to the lack of alkali metal, a loss of base sites at higher reduction temperatures, or extraction of alkali metals as in RRM − HCl, and a lack of a combination of weak and strong acid sites. Magnetite was clearly the active site for acetic acid ketonization since acetone yield and selectively increased with increasing magnetite levels in the RRM. The need for alkali metals in the red mud was most clearly demonstrated by the limited ketonization activity using the acid treated red mud in the presence of levoglucosan, although it had significantly higher surface area. Overall our results indicate the alkali metals (Ca, Na, K) should be maintained in the red mud and the reduction temperature controlled to, 1) generate magnetite with minimal levels of Fe°, 2) maintain both acid and base sites in the activated catalyst, and 3) reduce coking in the presence of levoglucosan.

## Acknowledgements

The authors graciously thank Joby Miller for her invaluable contributions of time and effort in analyzing materials and gaseous compositions. Support for this research and Justin Weber's MS in Biochemical Engineering was provided in part by a grant from the Southeastern Sun Grant Center with funds provided by the U.S. Department of Transportation Research and Innovative Technology Administration (DTOS59-07-G-00050) and a Strategic Research Initiative Grant from the College of Engineering at UGA. We also acknowledge the use of small portion of a USDA-NIFA Grant (Carbon Monolith Catalysts from Wood for Biobased Platform Chemicals: 2017-67021-26136) to support Nida Janulaitis (Undergraduate Research) and the $NH_3$-TPD analysis of the catalysts.

## Appendix A. Supplementary data

The following results are presented, 1) effect of magnetite levels on conversions, 2) carbon balances, 3) the reverse Mars-van Kevelen mechanism, 4) TGA analysis of recovered catalysts, 5) Surface area analysis of recovered catalysts, and 6) a proposed reaction pathway.

Supplementary material related to this article can be found, in the online version, at doi:https://doi.org/10.1016/j.apcatb.2018.08.061.

## References

[1] E. Karimi, A. Gomez, S. Kycia, M. Schlaf, Thermal Decomposition of Acetic and Formic Acid Catalyzed by Red Mud-Implications for the Potential Use of Red Mud as a Pyrolysis Bio-Oil Upgrading Catalyst, Energy Fuels 24 (4) (2010) 2747–2757.
[2] E. Karimi, I.F. Teixeira, A. Gomez, E. de Resende, C. Gissane, J. Leitch, M. Schlaf, Synergistic co-processing of an acidic hardwood derived pyrolysis bio-oil with alkaline Red Mud bauxite mining waste as a sacrificial upgrading catalyst, Appl. Catal. B 145 (2014) 187–196.
[3] E. Karimi, I.F. Tiexeria, L.P. Ribeiro, A. Gomez, R.M. Lago, G. Penner, M. Schlaf, Ketonization and deoxygenation of alkanoic acids and conversion of levulinic acid to hydrocarbons using a Red Mud bauxite mining waste as the catalyst, Catal. Today 190 (2012) 73–88.
[4] J.R. Kastner, R. Hilten, J.W. Weber, A.R. McFarlane, J.S.J. Hargreaves, V.S. Batra, Continuous catalytic upgrading of fast pyrolysis oil using iron oxides in red mud, RSC Adv. 5 (2015) 29375–29385.
[5] R. Hilten, J.W. Weber, J.R. Kastner, Continuous upgrading of fast pyrolysis oil by simultaneous esterification and hydrogenation, Energy Fuels 30 (2016) 8357–8368.
[6] S.H. Hakim, B.H. Shanks, J.A. Dumesic, Catalytic upgrading of the light fraction of a simulated bio-oil over CeZrOx catalyst, Appl. Catal. B 142-143 (2013) 368–376.
[7] R. Pestman, R.M. Koster, E. Boellard, A.M. Kraan, V. Ponec, Identification of the active sites in the selective hydrogenation of acetic acid to acetaldehyde on Iron oxide catalysts, J. Catal. 174 (1998) 142–152.
[8] R. Pestman, R.M. Koster, A. van Duijne, J.A.Z. Pieterse, V. Ponec, Reactions of carboxylic acids on oxides: 2. Bimolecular reaction of aliphatic acids to ketones, J. Catal. 168 (2) (1997) 265–272.
[9] D.E. Resasco, What Should We Demand from the Catalysts Responsible for Upgrading Biomass Pyrolysis Oil? J. Phys. Chem. Lett. 2 (2011) 2294–2295.
[10] K.O. Albrecht, R.A. Dagle, D.T. Howe, Characterization and Valorization of Aqueous Phases Derived From Liquefaction and Upgrading of Bio-oils, DOE Bioenergy Technologies Office (BETO), 2015 Project Peer Review. [Presentation].
[11] J.A. Bennett, C.M.A. Parlett, M.A. Isaacs, L.J. Durndell, L. Olivi, A.F. Lee, K. Wilson. Acetic Acid Ketonization over $Fe_3O_4/SiO_2$ for Pyrolysis Bio-Oil Upgrading, ChemCatChem 9 (2017) 1–8.
[12] S. Sushil, V.S. Batra, Catalytic applications of red mud, an aluminium industry waste: a review, Appl. Catal. B 81 (2008) 64–77.
[13] Y. Nakagawa, S. Liu, M. Tamura, K. Tomishige, Catalytic total hydrodeoxygenation of biomass-derived polyfunctionalized substrates to alkanes, ChemSusChem 8 (2015) 1114–1132.
[14] R.N. Olcese, M.M. Bettahar, B. Malamanc, J. Ghanbajac, L. Tibavizcoa, D. Petitjeana, A. Dufour, Gas-phase hydrodeoxygenation of guaiacol over iron-based catalysts. Effect of gases composition, iron load and supports (silica and activated carbon), Appl. Catal. B 129 (2013) 528–538.
[15] R.N. Olcese, G. Lardier, M. Bettahar, J. Ghanbaja, S. Fontana, V. Carro, A. Dufour, Aromatic chemicals by iron-catalyzed hydrotreatment of lignin pyrolysis vapor,

ChemSusChem 6 (2013) 1490–1499.
[16] F. Lu, B. Jiang, J. Wang, Z. Huang, Z. Liao, Y. Yang, Insights into the improvement effect of Fe doping into the $CeO_2$ catalyst for vapor phase ketonization of carboxylic acids, Mol. Catal. 444 (2018) 22–33.
[17] J. Weber, A. Thompson, J. Wilmoth, R.J. Gulotty Jr., J.R. Kastner, Coupling red-mud ketonization of a model bio-oil mixture with aqueous phase hydrogenation using activated carbon monoliths, Energy Fuels 31 (2017) 9529–9541.
[18] S. Narayanan, R. Unnikrishnan, Acetone hydrogenation over co-precipitated Ni/$Al_2O_3$, Co/$Al_2O_3$ and Fe/$Al_2O_3$ catalysts, J. Chem. Soc. - Faraday Trans. 94 (8) (1998) 1123–1128.
[19] V. Tishchenko, C. Meile, M.M. Scherer, T.S. Pasakarnis, A. Thompson, Fe2+ catalyzed iron atom exchange and re-crystallization in a tropical soil, Geochim. Cosmochim. Acta 148 (2015) 191–202.
[20] R.C.C. Costa, F.C.C. Moura, P.E.F. Oliveira, F. Magalhães, J.D. Ardisson, R.M. Lago, Controlled reduction of red mud waste to produce active systems for environmental applications: heterogeneous Fenton reaction and reduction of Cr(VI), Chemosphere 78 (2010) 1116–1120.
[21] N.M. Bennett, S.S. Helle, S.J.B. Duff, Extraction and hydrolysis of levoglucosan from pyrolysis oil, Bioresour. Technol. 100 (2009) 6059–6063.
[22] C.R. Vitasari, G.W. Meindersma, A.B. de Haan, Water extraction of pyrolysis oil: the first step for the recovery of renewable chemicals, Bioresour. Technol. 102 (2011) 7204–7210.
[23] J. Alvarez, R. Rosal, H. Sastre, F. Diez, Characterization and deactivation studies of an activated sulfided red mud used as hydrogenation catalyst, Appl. Catal. A Gen. 167 (2) (1998) 215–223.
[24] R. Chompoonut, R. Vithaya, A density functional study of propylene glycol conversion to Propanal and propanone of various acid-catalyzed reaction models: a water-addition effect, J. Comput. Chem. 26 (15) (2005) 1592–1599.
[25] R.W. Dorner, D.R. Hardy, F.W. Williams, H.D.K. Willauer, K and Mn doped iron-based $CO_2$ hydrogenation catalysts: detection of $KAlH_4$ as part of the catalyst's active phase, Appl. Catal. A Gen. 373 (2010) 112–121.
[26] J.C. Kuriacose, S.S. Jewur, Studies on the surface interaction of acetic acid on Iron oxide, J. Catalysis 50 (1977) 330–341.
[27] T.N. Pham, T. Sooknoi, S.P. Crossley, D.E. Resasco, Ketonization of carboxylic acids: mechanisms, catalysts, and implications for biomass conversion, ACS Catal. 3 (2013) 2456–2473.
[28] K. Parida, M.H.K. Kumar, Catalytic ketonisation of acetic acid over modified zirconia.1. Effect of alkali-metal cations as promoter, J. Mol. Catal. A Chem. 139 (1999) 73–80.
[29] A.G. Gayubo, A.T. Aguayo, A.A.R. Aguado, M. Olazar, J. Bilbao, Transformation of oxygenate components of biomass pyrolysis oil on a HZSM-5 zeolite. II. aldehydes, ketones, and acids, Ind. Eng. Chem. Res. 43 (2004) 2619–2626.
[30] M. Kaldstrom, N. Kumar, T. Heikkil, M. Tiitta, T. Salmi, D.Y. Murzin, Formation of furfural in catalytic transformation of Levoglucosan over mesoporous materials, ChemCatChem 2 (2010) 539–546.
[31] D.J. Nowakowski, J.M. Jones, Uncatalysed and potassium-catalysed pyrolysis of the cell-wall constituents of biomass and their model compounds, J. Anal. Appl. Pyrolysis 83 (2008) 12–25.